Hindawi
Advances in Multimedia
Volume 2023, Article ID 9796351, 1 page
https://doi.org/10.1155/2023/9796351

Retraction

Retracted: Multimedia Motion of Picking Robot Based on Cooperative Relationship of Matching Gradient Algorithm

Advances in Multimedia

Received 3 October 2023; Accepted 3 October 2023; Published 4 October 2023

This article has been retracted by Hindawi following an investigation undertaken by the publisher [1]. This investigation has uncovered evidence of one or more of the following indicators of systematic manipulation of the publication process:

(1) Discrepancies in scope
(2) Discrepancies in the description of the research reported
(3) Discrepancies between the availability of data and the research described
(4) Inappropriate citations
(5) Incoherent, meaningless and/or irrelevant content included in the article
(6) Peer-review manipulation

The presence of these indicators undermines our confidence in the integrity of the article's content and we cannot, therefore, vouch for its reliability. Please note that this notice is intended solely to alert readers that the content of this article is unreliable. We have not investigated whether authors were aware of or involved in the systematic manipulation of the publication process.

Wiley and Hindawi regrets that the usual quality checks did not identify these issues before publication and have since put additional measures in place to safeguard research integrity.

We wish to credit our own Research Integrity and Research Publishing teams and anonymous and named external researchers and research integrity experts for contributing to this investigation.

The corresponding author, as the representative of all authors, has been given the opportunity to register their agreement or disagreement to this retraction. We have kept a record of any response received.

References

[1] J. Han, "Multimedia Motion of Picking Robot Based on Cooperative Relationship of Matching Gradient Algorithm," *Advances in Multimedia*, vol. 2021, Article ID 4335552, 7 pages, 2021.

Hindawi
Advances in Multimedia
Volume 2021, Article ID 4335552, 7 pages
https://doi.org/10.1155/2021/4335552

Research Article

Multimedia Motion of Picking Robot Based on Cooperative Relationship of Matching Gradient Algorithm

Jinghai Han

Institute of Rail Transport, Nanjing Vocational Institute of Transport Technology, Nanjing, Jiangsu 211188, China

Correspondence should be addressed to Jinghai Han; hanjinghai@njitt.edu.cn

Received 9 August 2021; Accepted 15 October 2021; Published 9 December 2021

Academic Editor: Zhendong Mu

With the continuous development of social economy, robots gradually replace human beings in many aspects of auxiliary work, but it is worth noting that orderly, accurate, and safe operation is the reasonable form of robot movement. In view of the existing limitations, this study combines the gradient matching algorithm, by using a high-precision motion matching for the visual system, improves the automation precision, and, at the same time, picking fruit image smoothing and enhancement, achieves fruit edge feature extraction; the simulation experiments proved that matching the gradient algorithm is effective and can realize the visual and actions match together and support picking robot movement.

1. Introduction

With the continuous development of artificial intelligence, computer technology, and Internet of Things technology, more and more technologies have been introduced into various industries to improve work efficiency and change operation mode [1]. In terms of hardware development, robots can also be used to replace operations in previously unoperable environments. On the one hand, robots can be used to replace manpower for business operations, such as in extremely hot or cold environments. On the other hand, the robot can be integrated into the visual recognition system and endowed with corresponding artificial intelligence to achieve automatic operation with certain functions [2, 3]. Picking robot is a rapidly developing application. However, due to the complex environment faced by the picking, the image of the fruit is easily affected by external factors; more interference and positioning errors are brought to the robot, which increases the difficulty of picking and reduces the precision of picking [4–6].

For the traditional picking robot, it integrates the robot mechanical operation through visual analysis to realize the image discrimination first and then the process of picking. By using the robot's robot arm, the multicooperative operation is realized. Fruit-picking process of this way was affected by the image to obtain the factors of interference [7, 8]. In view of these limitations, this paper attempts to fuse the matching gradient algorithm, through the fusion of visual recognition and the picking robot, realize the image edge feature recognition, better cooperate with the robot for multiarm cooperative picking, achieve accurate and fast picking movement, and improve the precision and efficiency of picking.

2. Matching Gradient Algorithm

2.1. Matching Cost Calculation. For the matching gradient algorithm, the calculation of matching cost needs to be clarified first. Matching cost is the measure of similarity between the points with the same name relative to two images, and the definition of matching cost function can distinguish different images [9, 10]. Gradient is introduced into the calculation of matching cost, which can make the illumination influence little and has obvious and stable distinction to the noise of the image, so it can be widely used.

The gradient of the image is the first-order partial derivative of the image from the horizontal axis X and the vertical axis Y direction, which can be calculated by

$$\{g(x, y, t_0), g(x, y, t_1), \ldots, g(x, y, t_{N-1})\}, \quad (1)$$

where the gray value of the image is represented by I and the gradient vector of the image can be calculated using the corresponding template. Therefore, for the two images, the corresponding gradient value can be obtained, which can be expressed by the corresponding formula, such as $t_i - t_{i-1}$ and $G(x, y) = 1/2\pi\delta^2 \exp(-(x^2 + y^2)/2\delta^2)$.

As for the matching cost, it carries out quantitative calculation for the two images as follows:

$$G_m = \frac{\partial G}{\partial n} = n\nabla G. \quad (2)$$

The gradient matching cost function only considers the amplitude attribute of the image, but it cannot completely replace the basic information of the image. Therefore, phase information and amplitude information can be introduced at the same time to further improve the gradient matching cost function [11–13].

The corresponding gradient vector is expanded and defined in the horizontal and vertical axis directions to calculate the phase and amplitude of the image gradient vector, as shown in formulas (3) and (4):

$$n = \begin{bmatrix} \cos\theta \\ \\ \sin\theta \end{bmatrix}, \quad (3)$$

$$\nabla G = \begin{bmatrix} \dfrac{\partial G}{\partial x} \\ \\ \dfrac{\partial G}{\partial y} \end{bmatrix}, \quad (4)$$

where the gradient amplitude is expressed by m and the phase angle is expressed by φ. The function of matching cost can be obtained by fusion of amplitude value and phase angle as follows:

$$\nabla G. \quad (5)$$

In the formula, G_n and $G_n \cdot f(x, y)$, respectively, represent the gradient vector modules and phase angles corresponding to the color image channels R, G, and B, and a is the weighting coefficient. Further normalization to a single period, the specific calculation is shown as follows:

$$f(x) = \begin{cases} x, & \text{if } 0 \le x \le \pi, \\ 2\pi - x, & \text{if } \pi < x < 2\pi. \end{cases} \quad (6)$$

For the treatment of outliers, formula (7) is used in this paper for specific calculation and treatment:

$$\rho(x) = \frac{x^2}{x^2 + \sigma^2}. \quad (7)$$

As shown in Figure 1, when the input x is greater than the threshold range, the influence of the output value will decrease, and the matching cost gradually converges until it reaches 1. At the same time, parameter control is realized. In conclusion, no matter what the matching cost of the original input is, the output value is still less than 1 after the calculation of the quantitative function [14–16].

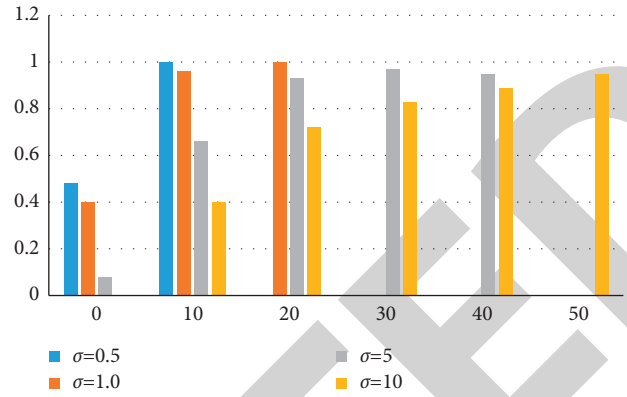

Figure 1: Geman–McClure function histogram.

2.2. Adaptive Window Generation. For an object, the recognition and matching of a single pixel are not enough, and its surrounding pixels need to be processed according to the matching cost function to improve the recognition degree and increase the recognition efficiency [17, 18]. Under the traditional matching algorithm, the recognition window is often fixed, and it is difficult to obtain high matching accuracy. Therefore, the core of the matching gradient algorithm in this paper is to set the adaptive window according to the spatial position of the adjacent pixels of the window. According to the matching pixels, it expands to form a cross region on the horizontal and vertical axis, and the length of the four arms of the robot is also adaptively adjusted according to the window.

Taking $E_y = \partial G/\partial y \cdot f(x, y)$ as an example, its discriminant criteria are as follows:

(1) $A(x, y) = \sqrt{E_x^2 + E_y^2}$

(2) $\theta = \arctan(E_x/E_y)$

(x_n^l, y_n^l, z_n^l) is the spatial distance difference between pixel (x_n^f, y_n^f, z_n^f) and p, (x_n^l, y_n^l, z_n^l) is the color difference, which is defined as (x_n^f, y_n^f, z_n^f). τ and L are the preset color threshold and distance threshold.

Therefore, it can be calculated by

$$\tau(l_p) = -\frac{\tau_{\max}}{L_{\max}} \times l_p + \tau_{\max}, \quad (8)$$

where $\begin{cases} J_\lambda(q)q = v \\ J_a(q)q = u \end{cases}$ and $[J_\lambda(q^l) + L(q^l)]\dot{q}^l - J_\lambda(q^f)\dot{q}^f = 0$ are the preset maximum color and distance thresholds, respectively, and $L(q^l) = \partial[O_0^n(q^l)r]/\partial q^l$ is the value of the current arm length. According to the above equation, $u^l = u^f$ is a linear function of $J_a(q^l)\dot{q}^l = J_a(q^f)\dot{q}^f$ and decreases

with the increase of $q^f = \begin{bmatrix} J_\lambda(qf) \\ [J_a(qf)]^{-1} \end{bmatrix}^{-1} \begin{bmatrix} J_\lambda(ql) + L(ql) \\ J_a(ql) \end{bmatrix} q^l$: when $l_p = 0$, the maximum value $\tau_{\max}$ is obtained. When $l_p = L_{\max}$, we take the minimum value 0.

The above determination criteria can be used to obtain the arm length $\{h_p^-, h_p^+, v_p^-, v_p^+\}$ size of pixel P, and then, we obtain the orthogonal cross region $H(p)$ and $V(p)$:

$$\begin{cases} H(p) = \{(x, y) | x \in [x_p - h_p^-, x_p + h_p^+], y = y_p\}, \\ V(p) = \{(x, y) | x \in x_p, y \in [y_p - v_p^-, y_p + v_p^+]\}. \end{cases} \quad (9)$$

Repeat the above process for each pixel Q in $V(p)$ along the vertical axis, obtain the horizontal support region $H(q)$ of Q, and combine all $H(q)$ to obtain the adaptive region of any pixel P in the image:

$$U(p) = \bigcup_{q \in V(p)} H(q). \quad (10)$$

2.3. Cost Aggregation. For traditional matching, which only consider the local area of the target graphics, in order to be able to obtain more reliable aggregation range, we need two images, respectively, for the consideration of local scope; the first is the function of the matching point corresponding definition, using the correlation method for adaptive region function, corresponding to generate the corresponding area. The superposed region is defined as the final local region, and the specific calculation can be obtained as

$$U_d(p) = \{(x, y) | (x, y) \in U(p), (x - d, y) \in U'(pd)\}. \quad (11)$$

On this basis, the original single pixel is matched and aggregated accordingly according to the superimposed region, and the total consumption within the region is calculated:

$$E(p, d) = \frac{1}{N} \sum_{q \in U_d(p)} e(q, d), \quad (12)$$

where the total number of pixels in the aggregation region is represented by N, and the point with the smallest matching cost is selected as the matching point within the parallax interval to select the parallax of point P and calculate the parallax:

$$d_p^0 = \arg \min_{0 \le d \le d_{\max}} E(p, d). \quad (13)$$

2.4. Parallax Elaboration. The parallax value corresponding to the maximum number of parallax occurrence is the optimal parallax value in statistical sense d_p^*; this optimal value is used to replace the initial parallax d_p^0 of pixel P; the specific calculation is as follows:

$$d_p^* = \arg \max_{0 \le d \le d_{\max}} \varphi_p(d). \quad (14)$$

3. Basketball Motion Capture System and Its Application in Motion Training of Picking Robot

The picking robot first needs to determine the location of the fruit, capture the corresponding fruit from the multimedia video, realize the autonomous positioning of the fruit, and then pick the fruit to realize the autonomous operation. The specific process is shown in Figure 2.

When designing the vision system of the picking robot, the target features of the fruit can be extracted according to the motion extraction technology of the basketball real-time video, and finally, the robot can realize the autonomous fruit positioning and autonomous operation.

3.1. Multimedia Motion and Image Edge Detection Matching of Picking Robot. For automatic fruit picking by the robot, the key lies in automatic positioning of fruit picking. Multimedia video motion feature acquisition and autonomous positioning are integrated to make clear that when picking targets, the picking robot will use features to acquire target features of fruit and complete the work of autonomous picking. Formula (15) is the relationship between multimedia image acquisition and time change in time series, which can be calculated specifically:

$$\{g(x, y, t_0), g(x, y, t_1), \ldots, g(x, y, t_{N-1})\}. \quad (15)$$

In the formula, $t_i - t_{i-1}$, B, T, and $G(x, y) = 1/2\pi\delta^2 \exp(-(x^2 + y^2)/2\delta^2)$, respectively, represent the image, the total number of frames, and the corresponding real-time moment and time interval when the image is collected.

When multimedia image collection is carried out, there will be strong interference in the process of image acquisition due to the fast movement. Therefore, it is necessary to reduce the noise of these images and use gradient algorithm to perform gradient processing on the image to enhance the edge features of the image and obtain the clear part. Therefore, it is necessary to set the corresponding gradient threshold to extract edge features, complete detection, and make clear the accurate positioning of image edges, as shown in Figure 3:

In the process of edge detection, the image needs to be processed, and the derivative is obtained. The specific calculation formula is shown as

$$G_m = \frac{\partial G}{\partial n} = n \nabla G, \quad (16)$$

where σ is the change of Gauss.

The first-order directional reciprocal calculation of the two-dimensional function is carried out according to the specific direction M. The specific calculation is shown in formulas (17)–(19):

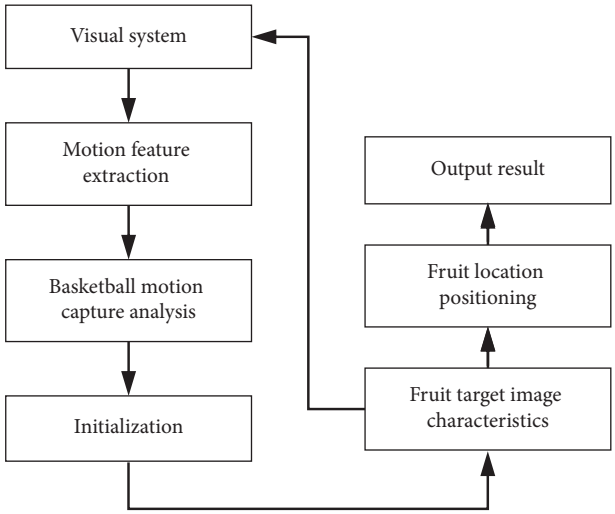

Figure 2: Basketball motion capture flowchart.

$$n = \begin{bmatrix} \cos\theta \\ \\ \sin\theta \end{bmatrix}, \tag{17}$$

$$\nabla G = \begin{bmatrix} \dfrac{\partial G}{\partial x} \\ \\ \dfrac{\partial G}{\partial y} \end{bmatrix}, \tag{18}$$

$$\nabla G, \tag{19}$$

where m and G_n represent direction vector and gradient vector and Theta is the angle of change.

The specific calculation of edge gradient is shown in formulas (20)–(23):

$$E_x = \frac{\partial G}{\partial x} \cdot f(x, y), \tag{20}$$

$$E_y = \frac{\partial G}{\partial y} \cdot f(x, y), \tag{21}$$

$$A(x, y) = \sqrt{E_x^2 + E_y^2}, \tag{22}$$

$$\theta = \arctan\left(\frac{E_x}{E_y}\right). \tag{23}$$

In the formula, $S(x,y)$ and ϕ are the edge strength and the normal vector at points in the real-time image (x,y), respectively, and a threshold is set for $H(x,y)$ to determine the maximum point of the local gradient of the image.

For picking on the edge of the target detection and recognition processes, as shown in Figure 4, the first is to obtain maximum fruit image edge extraction; secondly, set the corresponding threshold, save the value greater than the threshold, and set the saved value less than the threshold to 0. So far, the recognition of the edge of fruit images has provided a theoretical basis for the target positioning of fruit picking robots.

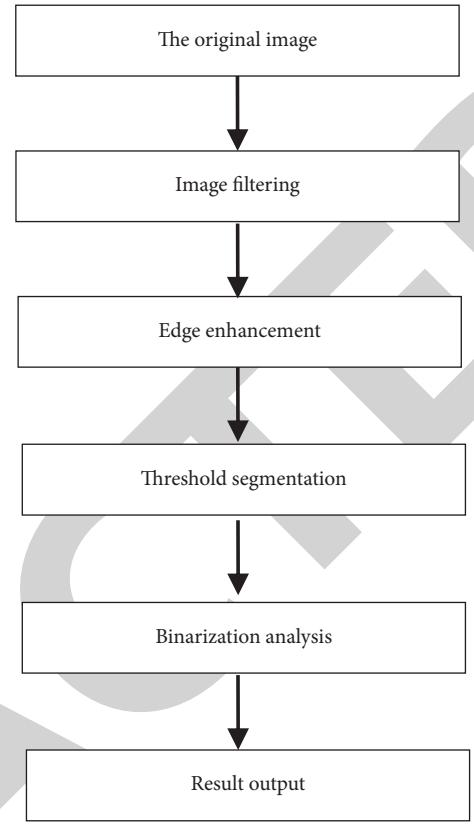

Figure 3: Flowchart of edge detection.

3.2. Motion Control Algorithm of Picking Robot Based on Constraint under Cooperative Relationship. After the picking robot completes the target picking, it is necessary to set the motion chain to carry out the collaborative processing of both arms. The specific process is as follows.

The two arms of the picking robot are divided into the active arm and the driven arm. (x_n^l, y_n^l, z_n^l) and (x_n^f, y_n^f, z_n^f) are used to represent the coordinate system at the end of the active arm and the driven arm, respectively. The vector from origin (x_n^l, y_n^l, z_n^l) to origin (x_n^f, y_n^f, z_n^f) is represented by K. Therefore, the position constraints and attitude constraints between the active arm and the driven arm are shown in formulas (24) and (25), respectively:

$$c\left(q^l\right) + O_0^n\left(q^l\right)k - c\left(q^f\right) = 0, \tag{24}$$

$$\left[n\left(q^l\right), s\left(q^l\right), a\left(q^l\right)\right]^T \left[n\left(q^f\right), s\left(q^f\right), a\left(q^f\right)\right] = W. \tag{25}$$

Based on the correlation between Jacobian $J(q) = [J_\lambda^T(q) J_a^T(q)]$ and $J(q)q = \begin{bmatrix} v \\ w \end{bmatrix}$, formula (26) is shown as

$$\begin{cases} J_\lambda(q)q = v, \\ J_a(q)q = u. \end{cases} \tag{26}$$

By the relationship of linear velocity, the ends of the two arms of the picking robot move together is shown as

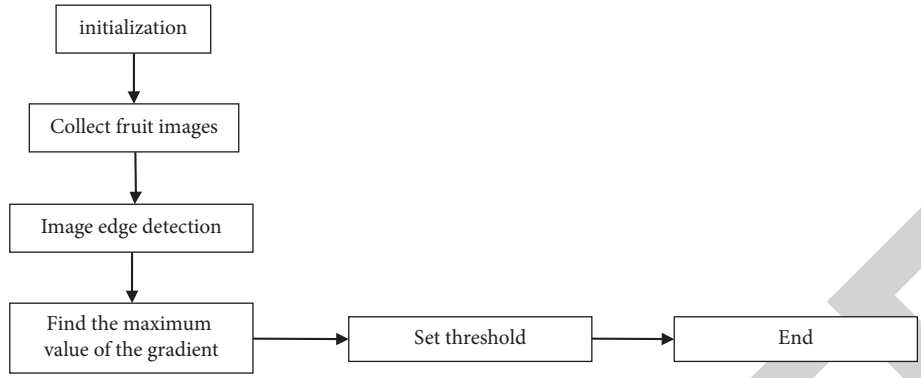

Figure 4: Picking robot edge detection and recognition process of the picking target.

$$\left[J_\lambda\left(q^l\right) + L\left(q^l\right)\right]\dot{q}^l - J_\lambda\left(q^f\right)\dot{q}^f = 0, \tag{27}$$

where $L(q^l) = \partial[O_0^n(q^l)r]/\partial q^l$.

When the picking robot moves in coordination, the angular velocity of the two arms is the same. Since there is no relative displacement at the ends of the two arms, that is, $u^l = u^f$, the calculation combined with formula (26) is shown as

$$J_a\left(q^l\right)\dot{q}^l = J_a\left(q^f\right)\dot{q}^f. \tag{28}$$

By combining equation (13) with equation (14), the correlation between the joint velocities of master and slave arms during cooperative movement is obtained:

$$q^f = \begin{bmatrix} J_\lambda(qf) \\ [J_a(qf)]^{-1} \end{bmatrix}^{-1} \begin{bmatrix} J_\lambda(ql) + L(ql) \\ J_a(ql) \end{bmatrix} q^l. \tag{29}$$

4. Visual Image Edge Detection of Picking Robot

According to the corresponding robot picking motion capture, multimedia video sequence analysis is realized. The specific image analysis is shown as follows:

$$\{g(x, y, t_0), g(x, y, t_1), \ldots, g(x, y, t_{N-1})\}. \tag{30}$$

In the process of image capture, the most important thing is the detection of the image edge. Through the edge detection of the image, the relevant hidden information is mined. The specific steps include

(1) Image filtering: through the collection of multimedia images, multimedia images need to be filtered because of the existence of various noise interferences

(2) Image enhancement: based on the gradient algorithm, the sharpness of the local blur of the image is processed and the edge of the image is detected

(3) Edge detection: by setting the edge points, the corresponding features are found, and then, the edge detection is carried out

(4) Fruit positioning: the precise position of the fruit edge is determined

During detection, the image is smoothed first, and then, the derivative of the image is obtained. The two-dimensional Gaussian function is shown as

$$G(x, y) = \frac{1}{2\pi\delta^2}\exp\left(-\frac{\left(x^2 + y^2\right)}{2\delta^2}\right). \tag{31}$$

The first directional derivative of $G(x,y)$ in a certain direction N is shown in formulas (32)–(34):

$$G_m = \frac{\partial G}{\partial n} = n\nabla G, \tag{32}$$

$$n = \begin{bmatrix} \cos\theta \\ \sin\theta \end{bmatrix}, \tag{33}$$

$$\nabla G = \begin{bmatrix} \dfrac{\partial G}{\partial x} \\ \dfrac{\partial G}{\partial y} \end{bmatrix}, \tag{34}$$

where n is the direction vector and ∇G is the gradient vector. The image $f(x,y)$ is convolved with G_n, and the direction of n is changed at the same time. When $G_n \cdot f(x, y)$ is maximized, the direction of edge detection is orthogonal to n. As shown in formulas (35)–(38),

$$E_x = \frac{\partial G}{\partial x} \cdot f(x, y), \tag{35}$$

$$E_y = \frac{\partial G}{\partial y} \cdot f(x, y), \tag{36}$$

$$A(x, y) = \sqrt{E_x^2 + E_y^2}, \tag{37}$$

$$\theta = \arctan\left(\frac{E_x}{E_y}\right). \tag{38}$$

5. Simulation Experiment and Analysis

In order to verify the match gradient algorithm, the multimedia sports feasibility of picking robot more collaborative relationships, choose an orchard of apple picking; the result is shown in Figure 5. From the results, the gradient matching algorithm is

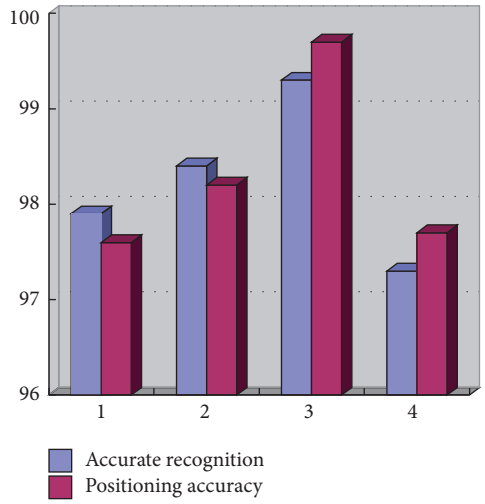

Figure 5: Picking performance test of picking robot (%).

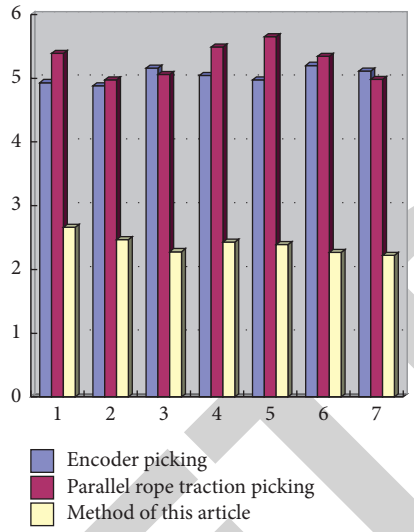

Figure 6: Time comparison results of image recognition with different methods (s).

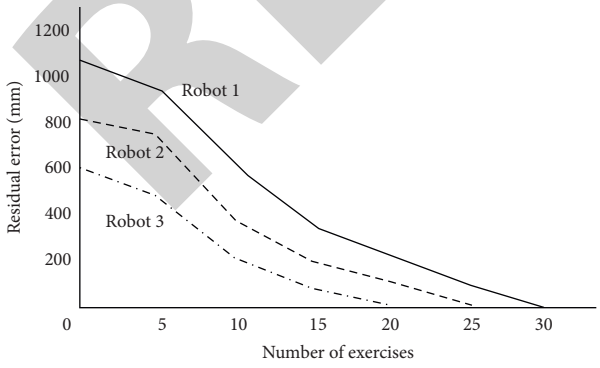

Figure 7: Control error test of the encoder-based control method.

10 times of picking graphics recognition accuracy of the mean, and the mean location accuracy reached 98.15% and 98.22%, respectively. It is proved that the matching gradient algorithm

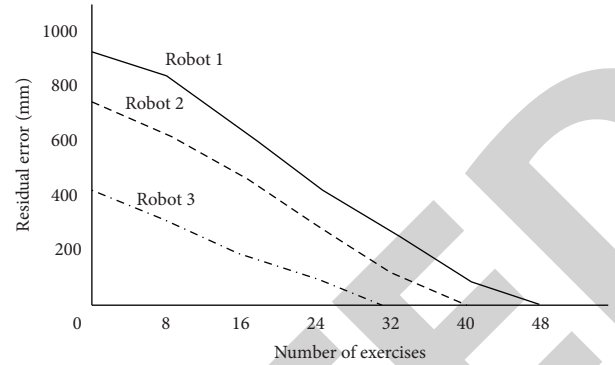

Figure 8: Control error test of the control method based on parallel rope traction.

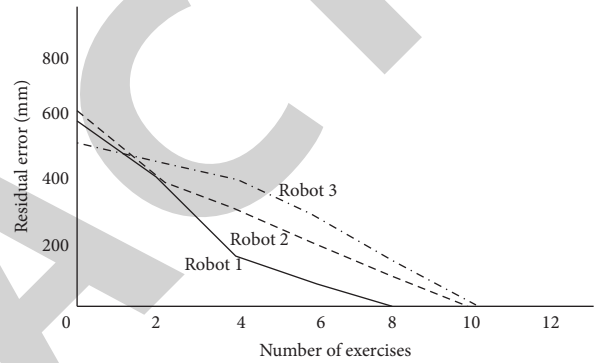

Figure 9: Control error test of this method.

can recognize and locate the image effectively, and the matching gradient algorithm is feasible to control the picking robot.

To test the efficiency and accuracy of gradient matching algorithm, simulation experiments in the same environment, the contrast gradient matching algorithm, and the other two kinds of the efficiency of the algorithm for image recognition, the result is shown in Figure 6. From the results, this paper identifies the fruit image and the time taken for an average of 2.46 seconds, while the other two methods of the consumed time is an average of more than 5.1 seconds. Therefore, in general, the matching gradient algorithm consumes less than half the time of the other two methods. Therefore, the matching gradient algorithm can effectively improve the image recognition efficiency of the picking robot.

By comparing Figures 7–9, the control accuracy under the same simulation environment is verified, respectively. The gradient matching algorithm only needs about 10 operations to minimize the error, while the other two methods need at least 30 operations. Therefore, the residual control of the gradient matching algorithm in this paper is significantly lower than the other two methods.

In order to verify the picking efficiency of this method, three different methods were used to test the picking efficiency.

As can be seen from Figure 10, the average time required by the matching gradient algorithm is about 30 seconds, while the other two methods are more than 40 seconds. Therefore, the matching gradient algorithm in this paper can greatly improve the efficiency of picking.

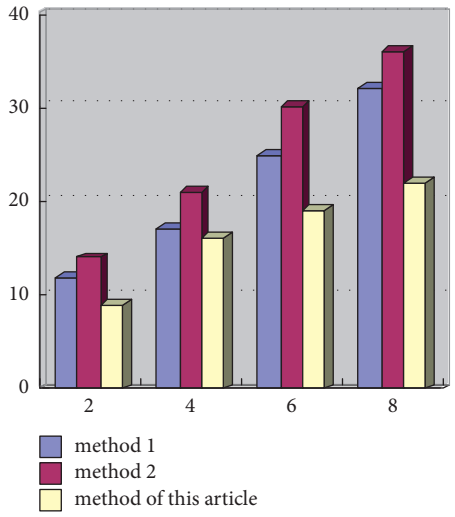

Figure 10: Comparison of picking efficiency of different methods.

6. Conclusions

The picking robot is a breakthrough attempt to replace artificial application in the field of agriculture, but precision and efficiency have always been the focus and difficulty of industry research. In this paper, in view of the limitations of the recognition accuracy of the picking robot, the matching gradient algorithm is fused, and the multimedia motion capture detection and feature extraction technology are referred to. The vision system of the picking robot is modified accordingly, and the accurate and fast fruit image recognition ability is obtained. The simulation results show that the matching gradient algorithm is effective and can identify the fruit target quickly, achieve the harvesting, and meet the requirements of high precision.

Data Availability

The data used to support the findings of this study are available upon request to the author.

Conflicts of Interest

The author declares no conflicts of interest.

References

[1] X. Hu, C. Wang, and T. Yu, "Design and application of visual system in the Agaricus bisporus picking robot," *Journal of Physics: Conference Series*, vol. 1187, no. 2, pp. 320–341, 2019.

[2] H. Z. Zhao, G. L. Yang, and C. Y. Chen, "Using 3D matching for picking and placing on UR robot," *Applied Mechanics and Materials*, vol. 870, pp. 289–294, 2017.

[3] L. Ye, J. Duan, Z. Yang, X. Zou, M. Chen, and S. Zhang, "Collision-free motion planning for the litchi-picking robot," *Computers and Electronics in Agriculture*, vol. 185, no. 2, pp. 106–121, 2021.

[4] X. Liu, "Dynamic simulation system using DOF picking robot," *The Open Automation and Control Systems Journal*, vol. 7, no. 1, pp. 1746–1751, 2015.

[5] H. Yang, L. Chen, M. Chen et al., "Tender tea shoots recognition and positioning for picking robot using improved YOLO-V3 model," *IEEE Access*, vol. 7, no. 3, pp. 180998–181011, 2019.

[6] Z. Yang, "Research on the application of rigid-flexible compound driven fruit picking robot design in realizing fruit picking," *Journal of Physics: Conference Series*, vol. 1952, no. 2, pp. 220–231, 2021.

[7] H. Chen and Z. Fang, "Design and research on the end actuator of tomato picking robot," *Journal of Physics: Conference Series*, vol. 13, no. 14, pp. 121–129, 2019.

[8] X. Hu, Z. Pan, and S. Lv, "Picking path optimization of agaricus bisporus picking robot," *Mathematical Problems in Engineering*, vol. 2019, no. 7, 16 pages, Article ID 897315, 2019.

[9] G. Lv, "High-speed parallel automatic control dynamic modeling of picking robot based on PLC," *IPPTA: Quarterly Journal of Indian Pulp and Paper Technical-A*, vol. 30, no. 6, pp. 796–802, 2018.

[10] Q. R. Zhang, R. H. Hu, and T. Z. Yu, "Design and implementation of cherry picking robot vision recognition system based on face recognition," *MATEC Web of Conferences*, vol. 63, no. 3, pp. 69–78, 2016.

[11] L. Wei, Y. Cui, and Z. Zhao, "Robust sliding mode control of cucumber picking robot based on the upper bound estimation," *Advance Journal of Food Science & Technology*, vol. 7, no. 3, pp. 177–182, 2015.

[12] F. Piltan, A. Taghizadegan, and N. B. Sulaiman, "Modeling and control of four degrees of freedom surgical robot manipulator using MATLAB/SIMULINK," *International Journal of Hospitality Information Technology*, vol. 8, no. 11, pp. 47–78, 2015.

[13] J. Han, L. Liu, and H. Zeng, "Design and implementation of intelligent agricultural picking mobile robot based on color sensor," *Journal of Physics: Conference Series*, vol. 1757, no. 1, pp. 12157–12168, 2021.

[14] T. Asaoka, K. Nagata, T. Nishi, and I. Mizuuchi, "Detection of object arrangement patterns using images for robot picking," *ROBOMECH Journal*, vol. 5, no. 1, pp. 986–992, 2018.

[15] R. Krug, T. Stoyanov, V. Tincani et al., "The next step in robot commissioning: autonomous picking & palletizing," *IEEE Robotics and Automation Letters*, vol. 1, no. 1, pp. 1–12, 2016.

[16] P. Jiang, Y. Ishihara, N. Sugiyama et al., "Depth image–based deep learning of grasp planning for textureless planar-faced objects in vision-guided robotic bin-picking," *Sensors*, vol. 20, no. 3, pp. 706–712, 2020.

[17] Y. Sato, K. Harada, N. Sakata, W. Wan, and I. G. Ramirez-Alpizar, "Two-stage robotic picking for randomly stacked objects with recognition difficulty," *Transactions of the JSME*, vol. 84, no. 861, pp. 1–8, 2018, in Japanese.

[18] A. Colomé and C. Torras, "A topological extension of movement primitives for curvature modulation and sampling of robot motion," *Autonomous Robots*, vol. 45, no. 3, pp. 1–11, 2021.